Autophagy

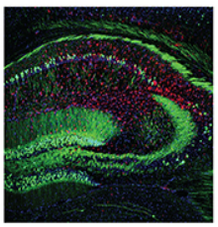

Autophagy

ISSN: 1554-8627 (Print) 1554-8635 (Online) Journal homepage: www.tandfonline.com/journals/kaup20

Signal-Sustained Imaging of Mitophagy with an Enzyme-Activatable Metabolic Lipid Labeling Probe

Xiaoxue Zou, Shixiong Wen, Lichun Xu, Lei Gao, Xunxiang Wang, Xiao Hu, Jiahuai Han & Shoufa Han

To cite this article: Xiaoxue Zou, Shixiong Wen, Lichun Xu, Lei Gao, Xunxiang Wang, Xiao Hu, Jiahuai Han & Shoufa Han (2024) Signal-Sustained Imaging of Mitophagy with an Enzyme-Activatable Metabolic Lipid Labeling Probe, Autophagy, 20:11, 2556-2570, DOI: 10.1080/15548627.2024.2367192

To link to this article: https://doi.org/10.1080/15548627.2024.2367192

AUTOPHAGY
2024, VOL. 20, NO. 11, 2556–2570
https://doi.org/10.1080/15548627.2024.2367192

Taylor & Francis
Taylor & Francis Group

RESEARCH PAPER

Signal-Sustained Imaging of Mitophagy with an Enzyme-Activatable Metabolic Lipid Labeling Probe

Xiaoxue Zou[a*], Shixiong Wen[b*], Lichun Xu[a], Lei Gao[a], Xunxiang Wang[a], Xiao Hu[a], Jiahuai Han[b*], and Shoufa Han[a,c]

[a]The Key Laboratory for Chemical Biology of Fujian Province, State Key Laboratory for Physical Chemistry of Solid Surfaces, The MOE Key Laboratory of Spectrochemical Analysis & Instrumentation, and Department of Chemical Biology, College of Chemistry and Chemical Engineering, Xiamen University, Xiamen, Fujian Province, China; [b]State key Laboratory of Cellular Stress Biology, School of Life Sciences, Xiamen University, Xiamen, Fujian Province, China; [c]Academician Workstation of Immune Cell Signal Transduction, School of Basic Medicine, Chongqing Medical University, Chongqing, China

ABSTRACT

Imaging of mitophagy is of significance as aberrant mitophagy is engaged in multiple diseases. Mitophagy has been imaged with synthetic or biotic pH sensors by reporting pH acidification en route delivery into lysosomes. To circumvent uncertainty of acidity-dependent signals, we herein report an enzyme-activatable probe covalently attached on mitochondrial inner membrane (ECAM) for signal-persist mitophagy imaging. ECAM is operated via ΔΨm-driven accumulation of Mito-proGreen in mitochondria and covalent linking of the trapped probe with azidophospholipids metabolically incorporated into the mitochondrial inner membrane. Upon mitophagy, ECAM is delivered into lysosomes and hydrolyzed by LNPEP/leucyl aminopeptidase, yielding turn-on green fluorescence that is immune to lysosomal acidity changes and stably retained in fixed cells. With ECAM, phorbol-12-myristate-13-acetate (PMA) was identified as a highly potent inducer of mitophagy. Overcoming signal susceptibility of pH probes and liability of ΔΨm probes to dissipation from stressed mitochondria, ECAM offers an attractive tool to study mitophagy and mitophagy-inducing therapeutic agents.

Abbreviations: Baf-A1, bafilomycin A_1; CCCP, carbonyl cyanide *m*-chlorophenylhydrazone; DBCO, dibenzocyclooctyne; ECAM, enzyme-activated probe covalently attached on mitochondrial inner membrane; GFP, green fluorescent protein; LAMP2, lysosomal associated membrane protein 2; LNPEP/LAP, leucyl and cystinyl aminopeptidase; PMA, phorbol-12-myristate-13-acetate; ΔΨm, mitochondrial transmembrane potential; RFP, red fluorescent protein; TPP, triphenylphosphonium.

ARTICLE HISTORY
Received 30 November 2023
Revised 28 May 2024
Accepted 8 June 2024

KEYWORDS
Enzyme activation; fluorescence-on; metabolic lipid labeling; mitophagy imaging; ph-independent fluorescence

Introduction

Mitophagy is a conserved cellular catabolic pathway by which superfluous or dysfunctional mitochondria are delivered to lysosomes for degradation [1–3]. Given the causal roles of dysfunctional mitochondria in diverse diseases [4–10], sensitive and reliable detection of mitophagy is of broad utility such as screening mitophagy inducers [11–13]. To date, lysosomal acidity has been widely exploited for mitophagy imaging, as evidenced by myriad synthetic pH sensors that are enriched in mitochondria by mitochondrial transmembrane potential (ΔΨm) and could fluoresce differently upon delivery into acidic lysosomes [14–20]. Similarly, autophagy has also been assessed by pH-reporting proteinaceous probes often consisting of a pair of fluorescent proteins with one optically quenched in acidic pH while the other not [21–24]. Albeit widely used, fluorescent protein-based imaging entails lengthy procedures such as cell transfection, and is hindered by high background signals that accumulate over time due to constitutive protein expression. Importantly, both synthetic and biotic pH sensors exhibit uncertainties such as disturbance or loss of optical readout in pH-elevated or permeabilized lysosomes, compromising reliable mitophagy detection in stressed cells or fixed cells.

Synthetic chemical probes are advantageous over proteinaceous ones as they are amenable to culture-to-use imaging and applicable to primary cells. This approach overrides the need for plasmid transfection and generation of a stable cell line expressing protein reporters. However, synthetic probes electrophoretically partitioned in mitochondria are prone to dissipation from mitochondria upon loss of ΔΨm [25–27], limiting their application to track depolarized or dysfunctional mitochondria. As such several methods have developed to immobilize synthetic probes in mitochondria ranging from covalent linking to intramitochondrial proteins [28–32], to self-assembly [33–35], and to *in situ* construction of multifunctional probes [36,37]. To circumvent signal disturbance of pH sensors by lysosomal pH alterations and as lysosomes contain diverse hydrolases, we envisioned that a ΔΨm probe activatable to enzymes in lysosomes could give mitophagy-reporting readout insusceptible to lysosomal pH alteration.

CONTACT Shoufa Han shoufa@xmu.edu.cn The Key Laboratory for Chemical Biology of Fujian Province, State Key Laboratory for Physical Chemistry of Solid Surfaces, The MOE Key Laboratory of Spectrochemical Analysis & Instrumentation, and Department of Chemical Biology, College of Chemistry and Chemical Engineering, Xiamen University, Xiamen, Fujian Province 361005, China; Jiahuai Han jhan@xmu.edu.cn Academician Workstation of Immune Cell Signal Transduction, School of Basic Medicine, Chongqing Medical University, Chongqing 400016, China
*Both authors contributed equally to this work.

Supplemental data for this article can be accessed online at https://doi.org/10.1080/15548627.2024.2367192.

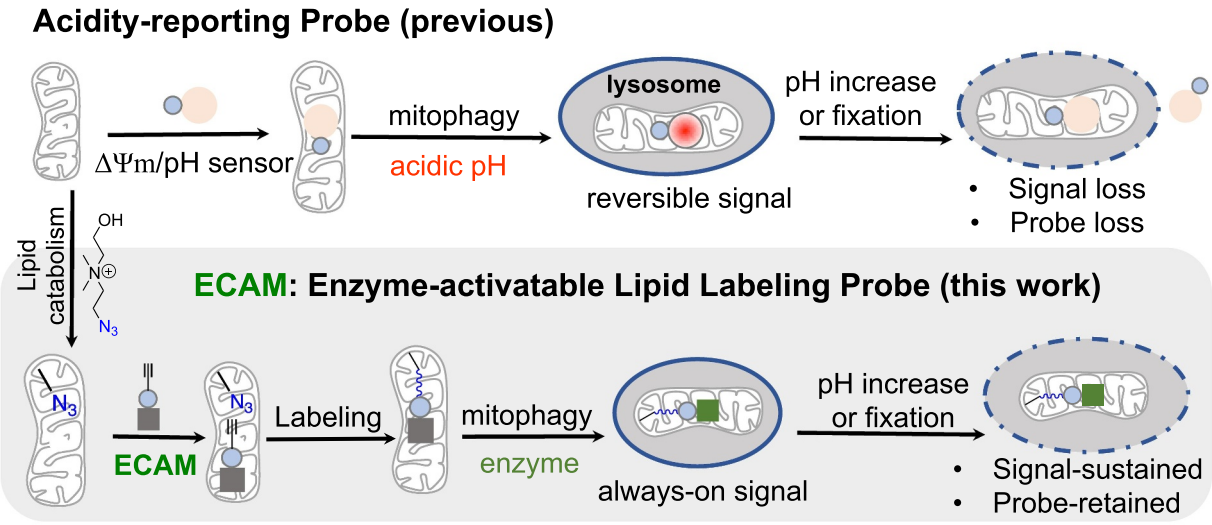

Figure 1. Schematic for signal-sustained mitophagy imaging with ECAM. (A) Liability of pH sensors to signal loss upon lysosomal pH elevation or cell fixation. (B) ECAM entails metabolic formation of azidophospholipids from ^{Az}choline, ΔΨm-mediated Mito-proGreen accumulation in mitochondria, and in situ covalent probe ligation with azidophospholipids in mitochondrial membrane. Upon mitophagy, ECAM undergoes LNPEP-triggered green fluorescence in lysosomes, yielding bright fluorescence that is immune to lysosomal pH changes and retained in fixed cells.

We herein report mitophagy imaging via an enzyme-activated probe covalently attached on mitochondrial inner membrane (ECAM) (Figure 1). The probe, Mito-proGreen, contains triphenylphosphonium (TPP) to promote probe accumulation in mitochondria [38–41], dibenzocyclooctyne (DBCO) for covalent ligation, and a profluorophore caged with L-leucine (Figure 2). ΔΨm-driven partition of Mito-proGreen in mitochondria enables *in situ* probe ligation with azidophospholipids metabolically installed on mitochondrial inner membrane. Upon mitophagy, ECAM is delivered into lysosomes and in turn activated by LNPEP/leucine aminopeptidase to give a rhodamine species that is covalently linked to lipid membrane and exhibits bright green fluorescence inert to local pH changes. Overcoming the liability of ΔΨm probes to loss from stressed mitochondria, ECAM enables fluorescence-sustained mitophagy imaging in live cells as well as fixed cells, and is used to discern mitophagy-inducing compounds.

Results and discussion

Synthesis and characterization of Mito-proGreen

To achieve an enzyme-activated mitophagy probe, we envisioned that the substrate entity serving as the optical trigger should be structurally small to minimally impede ΔΨm probe accumulation in mitochondria. Hence, we considered amino peptidases that remove a N-terminal amino acid. A panel of nonfluorescent derivatives of rhodamine 110 masked with various amino acids were individually cultured with HeLa, NIH-3T3, B16-F10 or MCF7 cells (Fig. S1 and S2A). Because removal of the amino acyl moiety by cognate amino peptidase yields highly fluorescent rhodamine 110 (Fig. S2A), these cells were assayed for intracellular green fluorescence by flow cytometry. This revealed that cells treated with leucylated rhodamine (probe **10**) exhibited the greatest fluorescence (Fig. S2B-E). In addition, green fluorescence from probe **10** was found to localize in lysosomes (Fig. S2F), consisting with proposed probe activation by LNPEP in lysosomes. As such LNPEP was targeted for ECAM.

To overcome the liability of ΔΨm probes to loss from dysfunctional mitochondria [25], ECAM was designed to covalently tether a ΔΨm probe to mitochondrial inner membrane. TPP could effectively ferry diverse cargos into mitochondria [38–41]. We hence synthesized Mito-proGreen comprised of TPP to target mitochondria, DBCO for covalent ligation with azidophospholipids, and an entity of leucylated rhodamine activatable to LNPEP Figure 2(A). As the control, Ac-Mito-proGreen was synthesized by acetylating amino group of Mito-proGreen Figure 2(A). Spectral analysis showed that Mito-proGreen and Ac-Mito-proGreen were nearly nonfluorescent at buffer of pH 8.0 and pH 4.5 Figure 2(B). Incubation of Mito-proGreen with LNPEP resulted in genesis of green fluorescence that intensified over time and as a function of LNPEP concentrations Figure 2(C,D). Furthermore, mass spectrometry analysis of the assay solution reveals a peak at 1077.087, corresponding to Mito-Green generated from Mito-proGreen activation by LNPEP (Fig. S2G). Moreover, formation of green fluorescence was dramatically inhibited by bestatin, a LNPEP inhibitor Figure 2(E). In contrast to Mito-proGreen, Ac-Mito-proGreen gave much weaker green fluorescence in the presence of LNPEP Figure 2(F), consistent with preferred LNPEP catalysis on Mito-proGreen over Ac-Mito-proGreen. Finally, we showed that green fluorescence is largely constant in the range of pH 4–9 Figure 2(G), supporting the applicability of ECAM for mitophagy imaging with fluorescence insusceptible to lysosomal pH changes. Combined, these results validate that Mito-proGreen could be activated by LNPEP to give green fluorescence independent of lysosomal acidity.

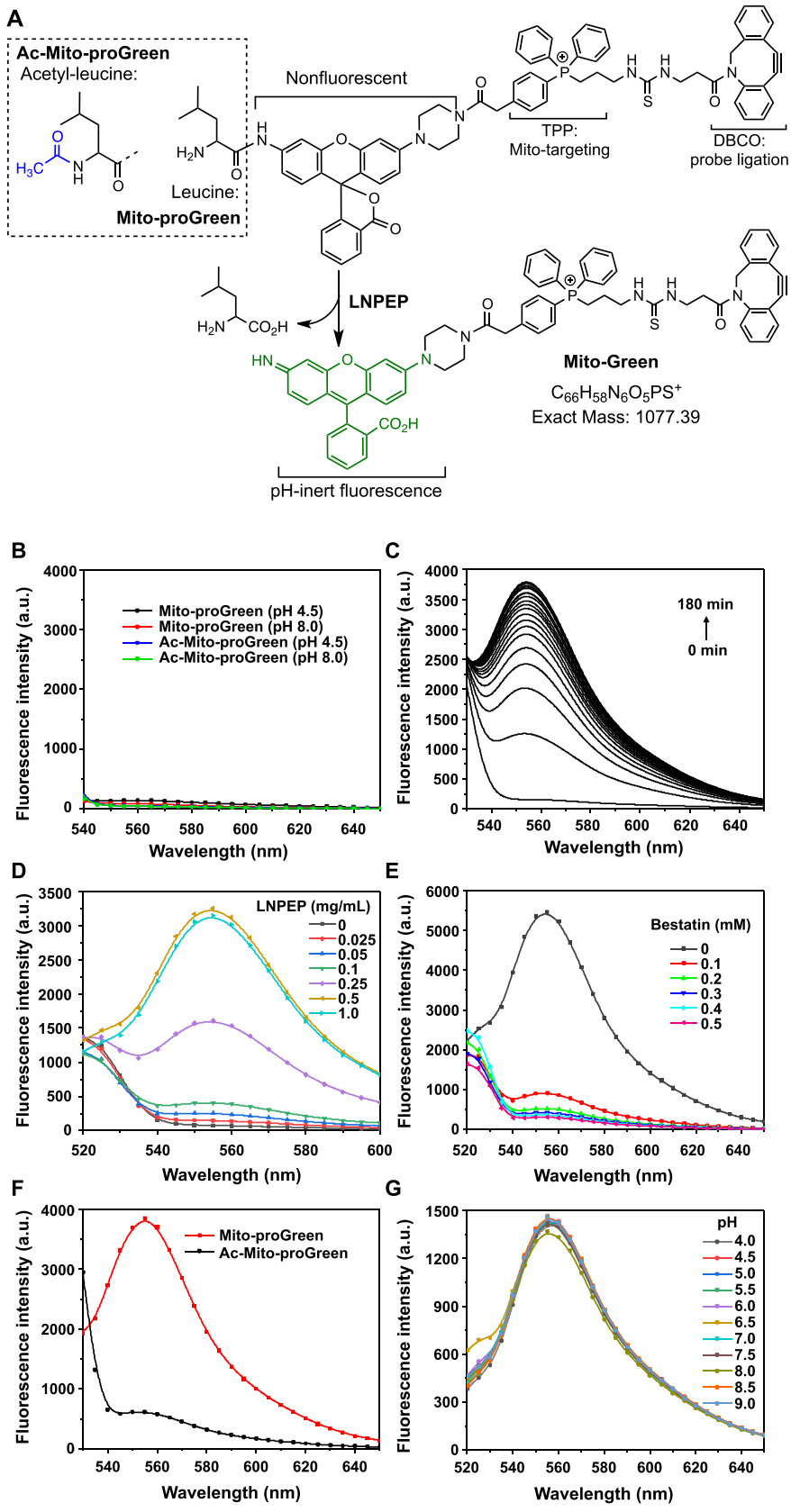

Figure 2. LNPEP-mediated fluorogenic activation of Mito-proGreen. (A) Chemical structures of Mito-proGreen and Ac-Mito-proGreen, and LNPEP catalysis on Mito-proGreen. (B) Fluorescence emission of Mito-proGreen (10 μM) and Ac-Mito-proGreen (10 μM) in phosphate-buffered saline (PBS, pH 4.5 or 8.0). (C) Temporal activation Mito-proGreen by LNPEP. Mito-proGreen (10 μM) was cultured with LNPEP (0.5 mg/mL) in PBS (10 mM, pH 7.4) for 0–180 min and then analyzed for fluorescence emission at indicated time points. (D) Dose-dependent activation of Mito-proGreen by LNPEP. Mito-proGreen (10 μM) was incubated with LNPEP (0–1.0 mg/mL) in PBS for 60 min and then assayed for fluorescence emission. (E) Bestatin inhibits Mito-proGreen activation by LNPEP. The solution of Mito-proGreen (10 μM) and LNPEP (0.5 mg/mL) was dosed with varied levels of bestatin (0–0.5 mM). The solution was incubated for 6 h and then detected for fluorescence emission. (F) Incapability of LNPEP to activate Ac-Mito-proGreen. Ac-Mito-proGreen (10 μM) was cultured with LNPEP (0.5 mg/mL) in PBS for 60 min prior to fluorescence analysis. (G) pH-inert green fluorescence of ECAM. The rhodamine fluorophore (10 μM) in PBS of pH 4.0–9.0 was analyzed for fluorescence emission using λ_{ex} = 520 nm.

Selectivity of Mito-proGreen for mitochondria

As Mito-proGreen is nonfluorescent, we assessed its selectivity for mitochondria via an intra-organelle probe ligation strategy [36]. Ligation of Mito-proGreen partitioned in mitochondria with a ΔΨm dye could yield a high molecular weight optical adduct that is stably trapped in mitochondria upon ablation of ΔΨm. Otherwise the ΔΨm dye would dissipate from depolarized mitochondria due to the absence of Mito-proGreen in mitochondria Figure 3(A). ^{Az}Red is a red-emissive ΔΨm dye specific for mitochondria Figure 3(A), but readily dissipates from mitochondria upon loss of ΔΨm [36,42]. HeLa cells were first cultured with ^{Az}Red and then cultured with varied concentrations of Mito-proGreen. These cells were further stressed with CCCP (carbonyl cyanide *m*-chlorophenylhydrazone) to abolish ΔΨm [43]. As expected, CCCP caused loss of red fluorescence from ^{Az}Red^{+} cells free of Mito-proGreen, a common feature of classical ΔΨm probes Figure 3(B). By contrast, ^{Az}Red was found to be maintained in cells co-stained with Mito-proGreen in a dose-dependent manner Figure 3(B,C). Furthermore, red signals exhibit a Pearson's correlation coefficient (PCC) of 0.81 and Manders' tM2 of 0.977 with MitoTracker Deep Red in CCCP-stressed ^{Az}Red^{+}/Mito-proGreen^{+} cells Figure 3(D). Colocalization of ^{Az}Red/Mito-proGreen with MitoTracker Deep Red specific for mitochondria shows accumulation of Mito-proGreen in mitochondria. In parallel, HeLa cells expressing green fluorescent protein (GFP)-tagged TOMM20,

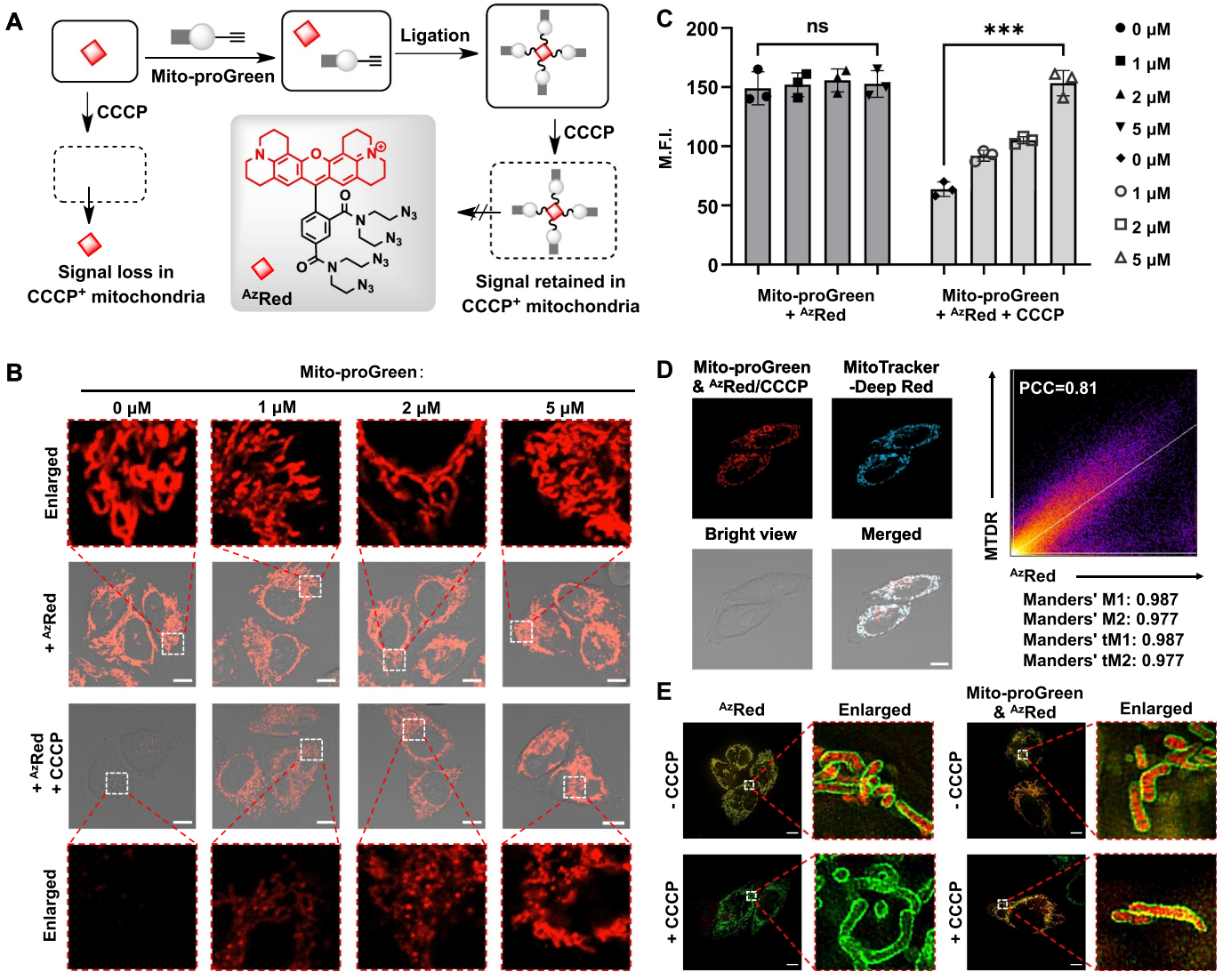

Figure 3. Selectivity of Mito-proGreen for mitochondria. (A) Schematic for ^{Az}Red retention in CCCP-stressed mitochondria by intra-organelle coupling with Mito-proGreen. (B) Mito-proGreen enables retention of ^{Az}Red in mitochondria. HeLa cells were stained with ^{Az}Red (0.2 μM, 1 h) and then with Mito-proGreen (0, 1, 2, 5 μM; 1 h) at 37°C. Cells were washed with PBS for three times and then stressed with CCCP (0, 30 μM; 30 min) before visualization by confocal microscopy. Scale bars: 10 μm. (C) Mean fluorescence intensity (M.F.I.) of ^{Az}Red^{+}/Mito-proGreen^{+} cells before and after CCCP treatment. Fluorescence intensity per cell was quantified by imagJ. The data are shown as the means ± SEM of three independent experiments, n = 20. ns, non-significant; ***p ≤ 0.001 (t test). (D) Colocalization of ^{Az}Red Mito-proGreen with MitoTracker Deep Red. ^{Az}Red^{+} Mito-proGreen^{+} HeLa cells were stained with MitoTracker Deep Red (0.2 μM, 15 min) and then imaged by confocal microscopy. Scale bars: 10 μm. (E) Retention of ^{Az}Red/Mito-proGreen in CCCP-stressed mitochondria. TOMM20-GFP^{+} cells were stained with ^{Az}Red (0.2 μM, 1 h) either alone or in combination with Mito-proGreen (2 μM, 1 h), stressed with CCCP (0, 30 μM; 1 h), and then imaged by SIM-Ultimate. Scale bars: 1 μm.

a mitochondrial membrane protein, were stained with ^{Az}Red either alone or in combination with Mito-proGreen and then stressed with CCCP. Super-resolution imaging showed that CCCP caused loss of red fluorescence enveloped by GFP-TOMM20 in ^{Az}Red^{+} cells but not ^{Az}Red^{+} Mito-proGreen^{+} cells Figure 3(E). Together, these findings show Mito-proGreen-dependent retention of ^{Az}Red in stressed mitochondria, further supporting accumulation of Mito-proGreen in mitochondria.

Mitophagy-dependent genesis of green fluorescence from ECAM

After confirming probe accumulation in mitochondria, we investigated whether Mito-proGreen alone could be used to image mitophagy [44,45]. First, wild type (WT) and *ATG5*-knock out (*ATG5*-KO) HeLa cells (Fig. S3A) were stained with Mito-proGreen and then maintained in probe-free medium for 6 h to allow basal autophagy. Green fluorescence was

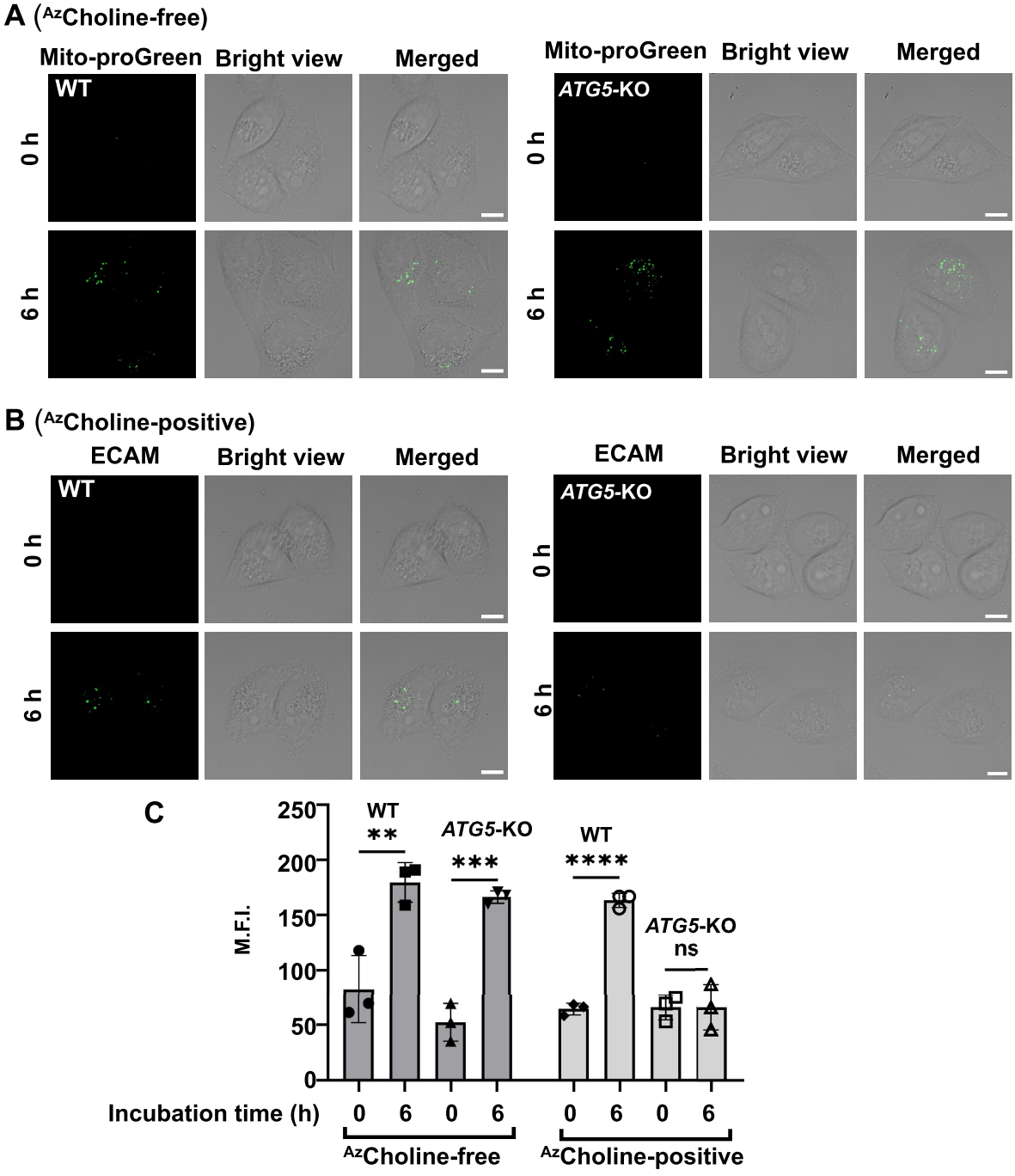

Figure 4. ECAM immobilizes Mito-proGreen in mitochondria. (A) Mito-proGreen was activated in mitophagy-deficient cells. WT and ATG5-KO HeLa cells were incubated with Mito-proGreen (2 μM, 1 h), respectively, and then maintained in fresh DMEM for 6 h prior to confocal microscopic analysis. (B) ECAM prevents non-mitophagic activation of Mito-proGreen. WT or ATG5-KO HeLa cells were cultured with ^{Az}choline (500 μM, 24 h) and then with Mito-proGreen (2 μM, 1 h). The cells were maintained in fresh DMEM for 6 h, and then visualized by confocal microscopy. (C) M.F.I of ECAM^{+} ATG5-KO HeLa cells as compared to Mito-proGreen^{+} ATG5-KO HeLa cells after 6 h culturing. M.F.I per cell was quantified by imageJ, data are presented as the means ± SEM of three independent experiments, n = 20. ns, non-significant; **p ≤ 0.01;***p ≤ 0.001; ****p ≤ 0.0001 (t-test). Scale bars: 10 μm.

observed in both cell lines Figure 4(A). As cells lacking ATG5 are defective in autophagosome formation, an essential step for mitophagy, green signals occurred in Mito-proGreen$^+$ *ATG5*-KO cells likely stem from probe leakage from mitochondria into lysosomes. This false-positive signal shows incapability of Mito-proGreen by itself to image mitophagy. Azido-containing phospholipids could be metabolically formed from exogenous ^{Az}choline and then distribute to biological membranes [46]. The azido moiety offers a chemical handle for bioorthogonal ligation on biological membrane [47,48]. To apply ECAM for mitophagy, we first performed in vitro reaction found that Mito-proGreen readily combined with ^{Az}choline to give the desired adduct as confirmed by HPLC and high-resolution mass spectrometry (Fig. S4). Next, we treated WT and *ATG5*-KO HeLa cells with ^{Az}choline for 24 h to allow biosynthesis of azidophospholipids, and then with Mito-proGreen for 1 h. These Mito-proGreen$^+$ ^{Az}choline$^+$ (referred to as ECAM$^+$) cells were further maintained for 6 h in probe-free medium. To our delight, green fluorescence was observed in ECAM$^+$ WT cells but not in *ATG5*-KO ECAM$^+$ cells Figure 4(B,C). Contrasting the fluorescence generated in Mito-proGreen$^+$ *ATG5*-KO cells Figure 4(A,C), the lack of such signals in ECAM$^+$ *ATG5*-KO cells deficient in mitophagy rules out the presence of extra-mitochondrial Mito-proGreen that could be delivered into lysosomes by general autophagy. This further consolidates the selectivity of Mito-proGreen for mitochondria. Combined, these data demonstrate that metabolic lipid labeling effectively immobilizes Mito-proGreen in mitochondria and prevents non-mitophagic false-positive signals.

As ECAM prevents non-mitophagic probe activation, we assessed ECAM by starving WT or *ATG5*-KO HeLa cells in Hanks' balanced salt solution (HBSS) free of amino acids for 6 h to induce autophagy (Fig. S3B). Relative to null fluorescence in ECAM$^+$ control cells free of starvation, starved ECAM$^+$ WT cells displayed intense green fluorescence whereas such signals were dramatically inhibited in ECAM$^+$ *ATG5*-KO cells Figure 5(A,B). Similar effects occurred in *ATG9A*-KO cells and *ATG7*-KO cells Figure 5(A,B), Figure S3A. As ATG5, ATG7 and ATG9A are critical regulators of mitophagy, starvation-triggered fluorescence in WT cells but not in cells deficient in ATG5, ATG7 or ATG9A proves mitophagy-specific activation of ECAM. We next compared ECAM in HeLa cells overexpressing Flag-tagged PRKN (referred to as *PRKN*$^+$ HeLa cells) with *PRKN*-KO HeLa cells as well as WT HeLa cells that exhibit low levels of mitophagy due to lack of PRKN (Fig. S3C) [49]. Upon treatment with CCCP, an inducer of mitophagy [50], robust green signals were induced in *PRKN*$^+$ cells but not in WT cells Figure 5(C,D). Given the role of PRKN in promoting mitophagy [49], this further cements the fidelity of ECAM for mitophagy.

To ascertain the applicability of ECAM for dysfunctional mitochondria, Mito-proGreen$^+$ or ECAM$^+$ HeLa cells were stressed with CCCP to depolarize mitochondria and then starved to induce mitophagy. CCCP treatment prior to starvation decreased green fluorescence in Mito-proGreen$^+$ cells but not in ECAM$^+$ cells Figure 5(E,F), demonstrating incapability of Mito-proGreen alone to track stressed mitochondria and the utility of ECAM to track stressed mitochondria in mitophagy. Independently, CCCP-induced mitophagy in these assays was confirmed by western blotting on ratios of LC3A/LC3B (Fig. S3D). Taken together, these results established the fidelity of ECAM for mitophagy.

Finally, we pinpointed subcellular location of ECAM-conferred green signals by staining ECAM$^+$ HeLa cells with LysoTracker Red specific for lysosomes. We observed colocalization of green fluorescence of ECAM with LysoTracker Red after starvation (Fig. S5A). In addition, we applied ECAM to HeLa cell expressing LAMP2 (lysosomal associated membrane protein 2) fused with red fluorescent protein (RFP) and found that cell stravation gave rise to both green- and LAMP2-positive deposits (Fig. S5B). These lysosome-specific green signals are in line with starvation-enabled delivery of ECAM$^+$ mitochondria into lysosomes, further consolidating the fidelity of ECAM for mitophagy by green fluorescence.

LNPEP-triggered green fluorescence of ECAM

To investigate the role of LNPEP in ECAM imaging, we stained ^{Az}choline$^+$ HeLa cells with Ac-Mito-proGreen, a poor substrate of LNPEP Figure 2(F), and then starved these cells. In contrast to ECAM$^+$ cells, starvation yields no detectable fluorescence in Ac-Mito-proGreen$^+$ ^{Az}choline$^+$ cells Figure 6(A). We next administered ECAM in HepG2 and A549 cells, the former expressing higher levels of lysosomal LNPEP than the latter [51]. Much brighter fluorescence was induced by starvation in HepG2 cells over A549 cells Figure 6(B). These results show LNPEP-mediated fluorogenic activation of Mito-proGreen instead of Ac-Mito-proGreen Figure 2(A).

To test whether ECAM-based mitophagy readout is immune to interference of lysosomal pH variation, ECAM$^+$ HeLa cells were starved in HBSS to allow genesis of mitophagy-reporting green fluorescence, and then treated with bafilomycin A_1 (Baf-A1). Baf-A1 is a potent inhibitor of V-ATPase and effectively neutralizes lysosomes [52]. It was shown that Baf-A1 caused no changes on the magnitude of green fluorescence in ECAM$^+$ cells Figure 6(C), reflecting lysosomal acidity-independent mitophagy-reporting signal of ECAM. For comparison, mitophagy was also imaged with an acidity-reporting probe (^{DBCO}RC-TPP) pre-anchored on mitochondrial inner membrane [37]. The mitophagy-reporting red fluorescence diminished upon Baf-A1 treatment Figure 6(C), showing signal vulnerability of this mitophagy probe to lysosomal pH changes. Cell fixation is beneficial for statistical and long-term analysis of mitophagy [53]. As cell fixation eliminates proton gradient across lysosomal membrane, acidity-reporting mitophagy probes are incompetent in fixed cells. To assess the applicability of ECAM in fixed cells, starved ECAM$^+$ HeLa cells were fixed with paraformaldehyde. We observed green signals in fixed ECAM$^+$ cells whereas such signals vanished in cells treated with Mito-proGreen alone Figure 6(D). This shows that covalent attachment of Mito-proGreen to mitochondrial membrane enables re)ention of green fluorescence after cell fixation. Combined, these results revealed that mitophagy-reporting fluorescence of ECAM was inert to lysosomal pH changes and well

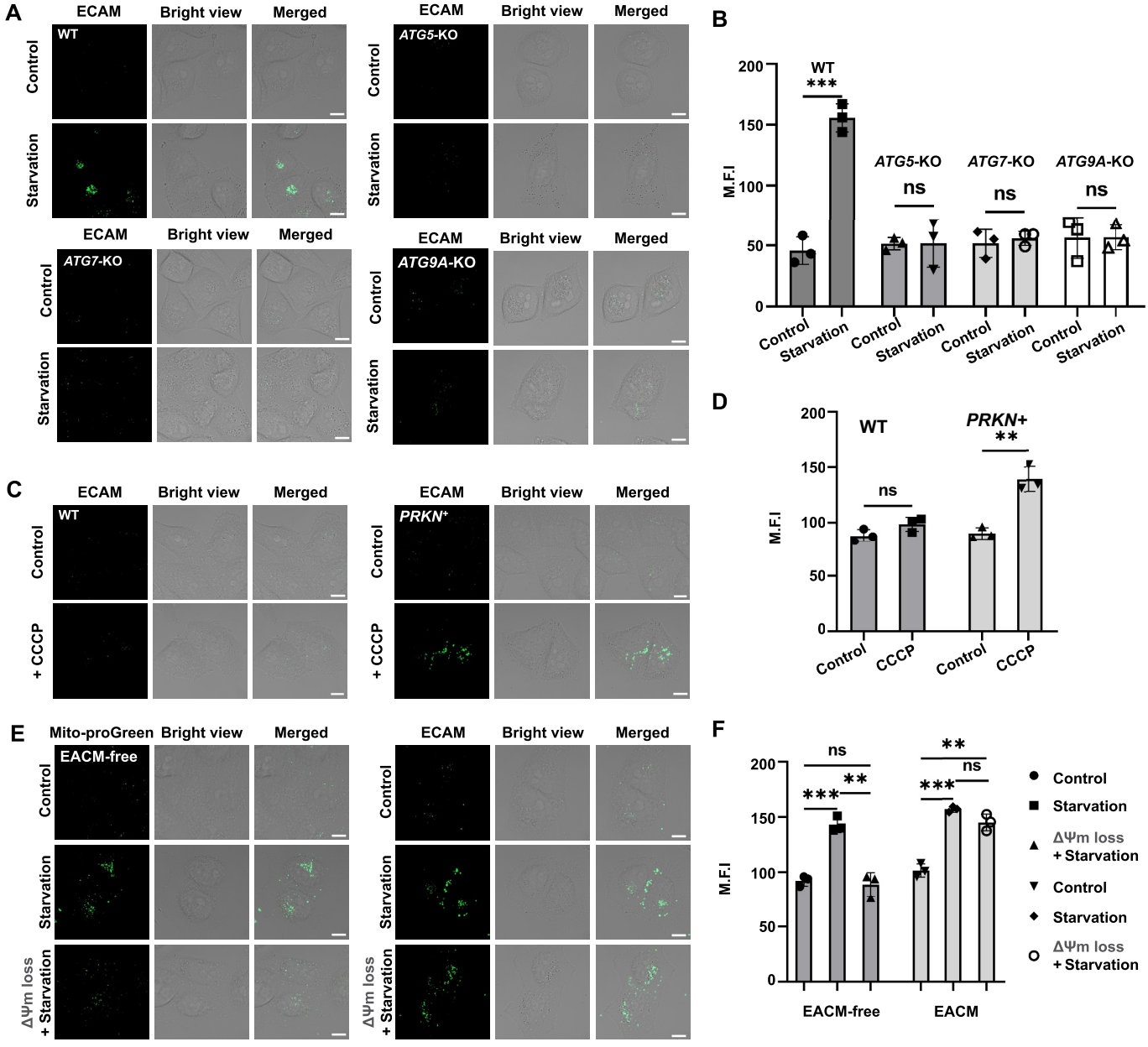

Figure 5. Fidelity of ECAM for mitophagy. Inhibited ECAM activation in ATG5-KO, ATG9A-KO, and ATG7-KO cells upon starvation. WT, ATG5-KO, ATG9A-KO and ATG7-KO HeLa cells pre-labeled with ECAM were maintained for 6 h in HBSS deficient in amino acids or DMEM (control). These cells were imaged by confocal microscopy (A) and measured for M.F.I. (B). PRKN enhances ECAM activation in mitophagy. ECAM$^+$ WT or ECAM$^+$ PRKN$^+$ HeLa cells were independently incubated with CCCP (0 or 10 μM, 6 h). The cells were visualized by confocal microscopy (C) and then quantified for M.F.I. (D). ECAM enables mitophagy imaging of stressed mitochondria. Mito-proGreen$^+$ or ECAM$^+$ HeLa cells were incubated with CCCP (0, 30 μM; 6 h) in DMEM, starved for 6 h in HBSS and then imaged by confocal microscopy (E) or measured for M.F.I. (F). M.F.I. per cell was quantified by imageJ. Data are presented as means ± SEM of three independent experiments. n = 20. ns, non-significant; **p ≤ < 0.01, ***p < 0.001 (t-test). Scale bars: 10 μm.

retained in fixed cells, two features beneficial for quantitation of mitophagy. Lastly, we monitored mitophagy in ECAM$^+$ WT HeLa cells as a function of starvation time. We identified green signals formed at 2 h post-starvation, increased over time and became highly bright at 6 h post-incubation (Fig. S6). Similar patterns were also observed on CCCP-triggered mitophagy in ECAM$^+$ *PRKN*$^+$ HeLa cells (Fig. S6). These results suggest that there is a lag of 4 hours between delivery of the probe into the lysosomes and genesis of intense fluorescence as it takes some time for leucine moiety to be cleaved from ECAM by LNPEP.

Discern of mitophagy induced by pharmacological agents

As accumulation of dysfunctional mitochondria is a hallmark of a number of human diseases [54], mitophagy inducers or enhancers are of therapeutic potentials [55]. Hence ECAM was implemented in *PRKN*$^+$ HeLa cells to discern mitophagy induced by rapamycin, etoposide, CCCP, rotenone, and oligomycin. Rapamycin is an immunosuppressing drug capable of enhancing autophagy through inhibition of MTOR [56–59] while etoposide is an anti-cancer agent causing mitochondrial dysfunction [60,61]. Rotenone inhibits mitochondrial complex I, and oligomycin suppresses mitochondrial ATP

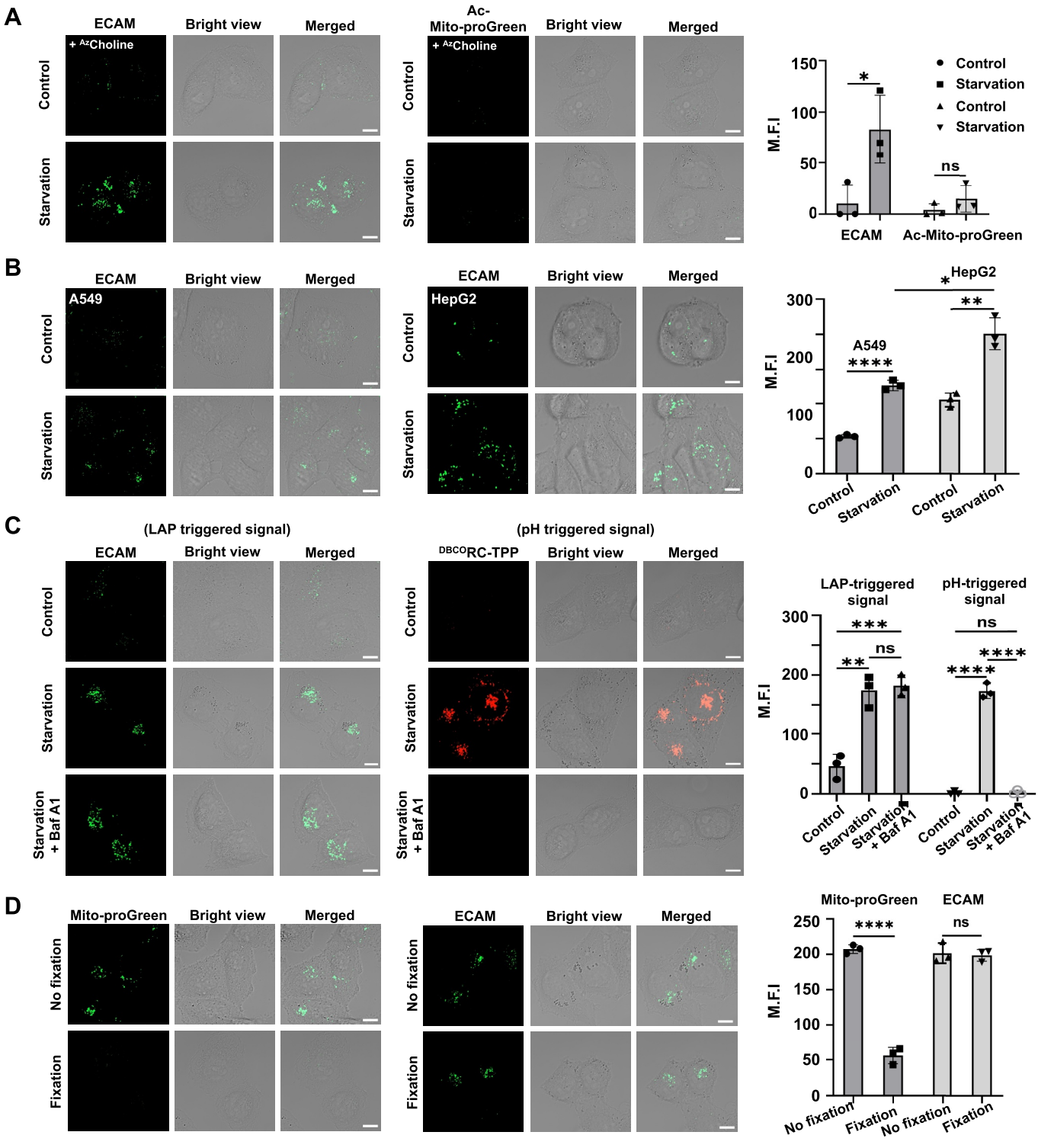

Figure 6. Fluorogenic activation of ECAM by LNPEP. (A) Incapability of Ac-Mito-proGreen for mitophagy imaging. ^{Az}Choline^{+}/Ac-Mito-proGreen^{+} or ECAM^{+} cells were starved in HBSS for 6 h. The cells were imaged by confocal microscopy. (B) Correlation of LNPEP abundance with mitophagy-specific green fluorescence. ECAM^{+} A549 cells and ECAM^{+} HepG2 cells were independently starved in HBSS for 6 h and then visualized by confocal microscopy. (C) Acidity-independent green fluorescence of ECAM. ECAM^{+} HeLa cells or ^{Az}choline^{+}/^{DBCO}RC-TPP^{+} HeLa cells were starved in HBSS spiked without or with Baf-A1 and then analyzed by confocal microscopy. (D) Retention of green fluorescence from ECAM in fixed cells. ECAM^{+} or Mito-proGreen^{+} HeLa cells were starved in HBSS and then treated with paraformaldehyde at room temperature for 15 min. The cells were washed three times with PBS, visualized by confocal microscopy and measured for M.F.I. quantified by imageJ. Data are representative of three independent experiments and values are expressed in means ± SEM. n = 20. ns, non-significant; *p ≤ 0.05 **p ≤ 0.01, ***p ≤ 0.001, ****p ≤ 0.0001 (t-test). Scale bars: 10 μm.

synthase. Confocal microscopy imaging revealed obvious mitophagy induced by these agents dosed at 10 μM Figure 7 (A). Quantitative analysis on intracellular fluorescence intensity reveals the levels of mitophagy promoted by rotenone > etoposide > CCCP > rapamycin > oligomycin Figure 7 (C). To assess the routes underlying mitophagy induced by

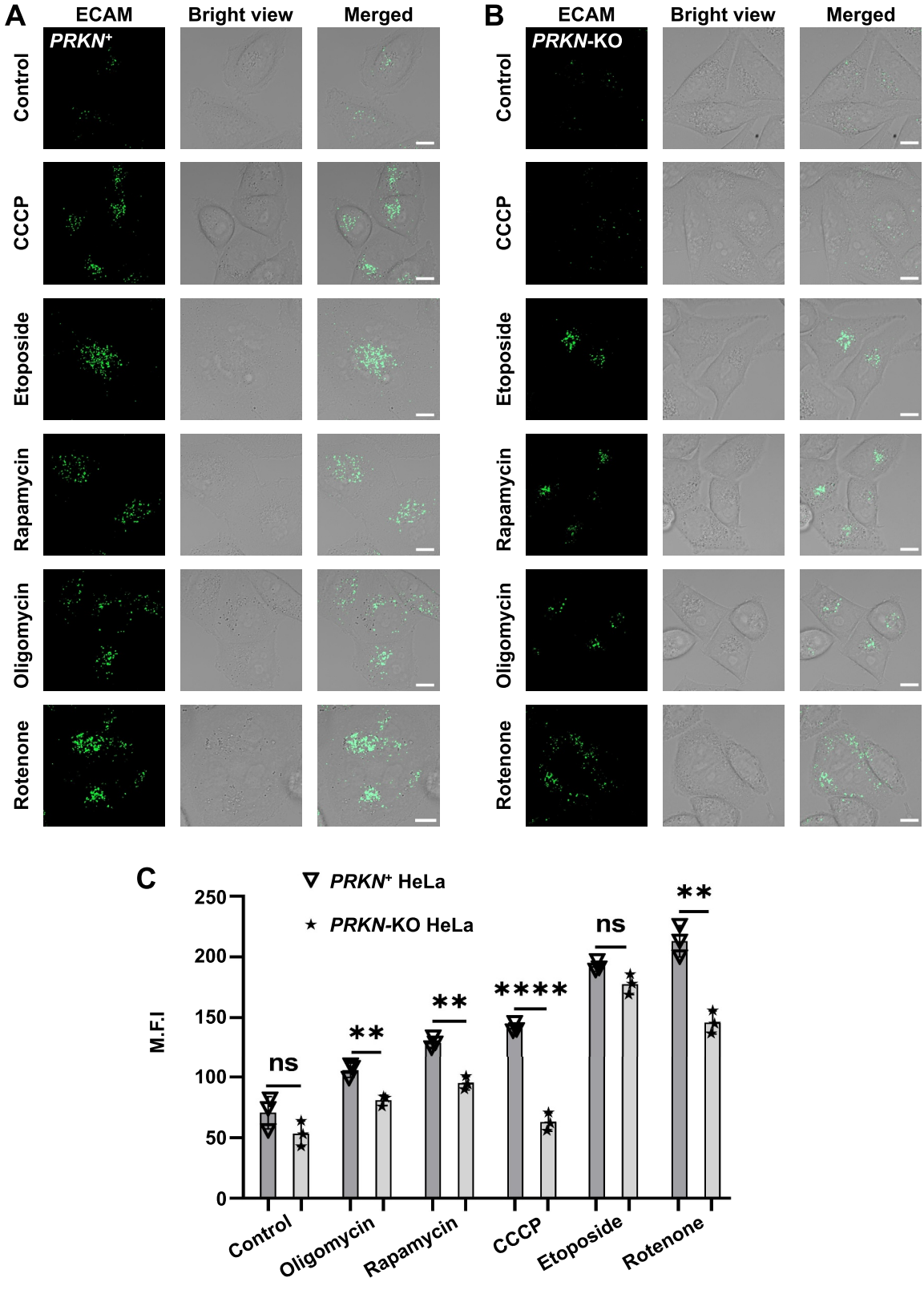

Figure 7. ECAM discerns mitophagy inducers. ECAM$^+$ PRKN$^+$ (A) or ECAM$^+$ PRKN-KO HeLa cells (B) were independently cultivated with CCCP (10 μM), etoposide (10 μM), rapamycin (10 μM), rotenone (10 μM), oligomycin (10 μM), or no addition (control) for 6 h in DMEM and then imaged by confocal microscopy. (C) Intracellular fluorescence intensity of drug-treated ECAM$^+$ cells. M.F.I. was determined by imageJ. Data are presented as means ± SEM of three independent experiments. n = 20. ns, non-significant; *p ≤ 0.05 **p ≤ 0.01, ***p ≤ 0.001, ****p ≤ 0.0001 (t-test). Scale bars: 10 μm.

these agents, we applied ECAM to *PRKN*-)KO cells. Relative to *PRKN*$^{+}$ cells, *PRKN*-KO cells displayed significantly suppressed mitophagy induced by CCCP whereas etoposide gave no obvious changes, with the rest causing comparatively smaller decrease in mitophagy Figure 7(B,C). This demonstrates that CCCP could induce mitophagy in part through the PINK1-PRKN pathway and in part PRKN-independent pathways whereby etoposide-induced mitophagy is largely PRKN-independent. Combined, these data showed that ECAM could distinguish PRKN-dependent and -independent mitophagy following mitochondrial uncoupling or other bioenergetic challenges to mitochondria.

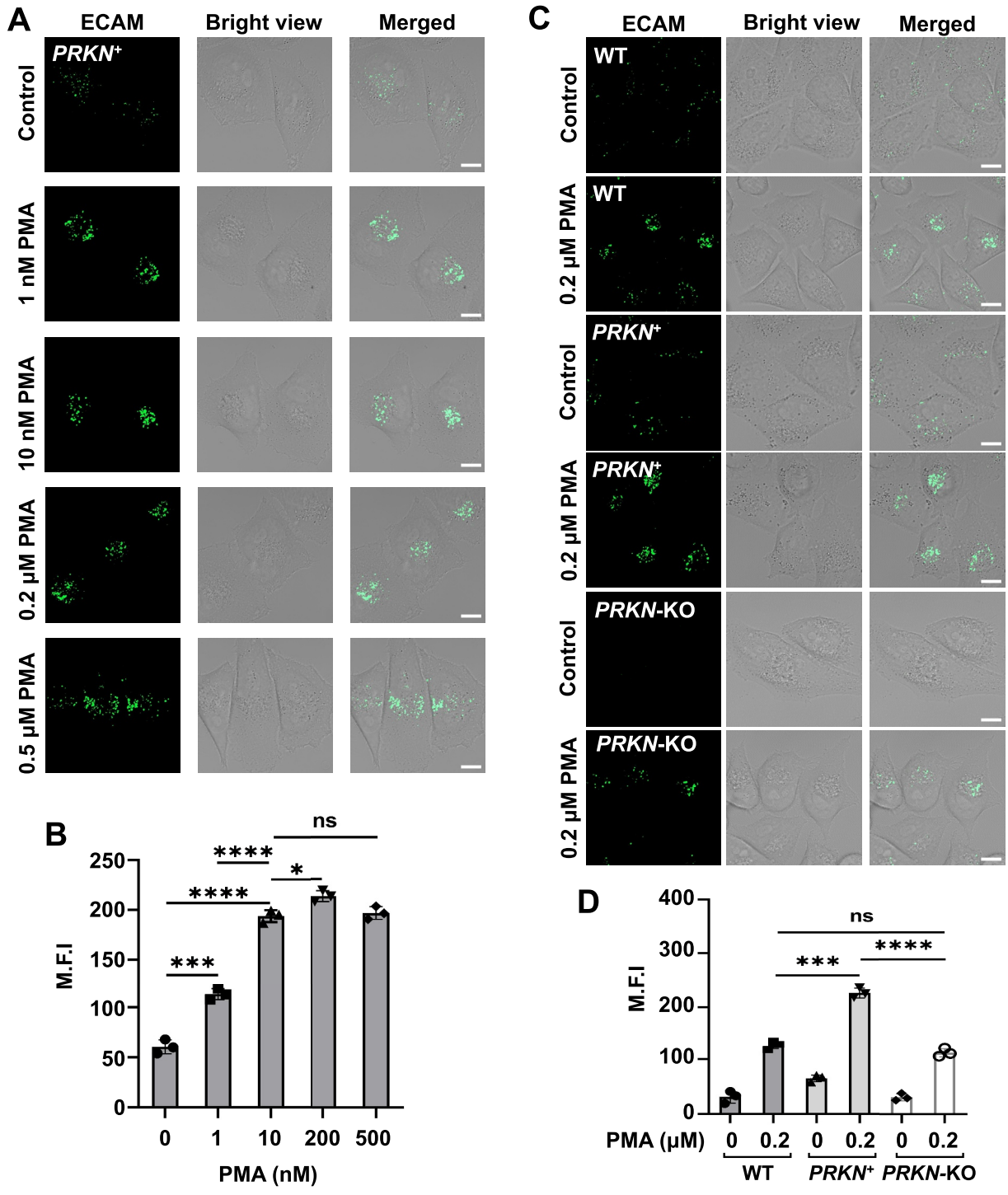

Figure 8. Identification of PMA as a potent mitophagy inducer. Mitophagy induced by PMA in PRKN^{+} HeLa cells. ECAM^{+} PRKN^{+} HeLa cells were cultivated in DMEM supplemented with PMA (0, 1 nM, 10 nM, 0.2 μM, or 0.5 μM) for 6 h. The cells were visualized by confocal microscopy (A) and measured for intracellular fluorescence intensity. (B). Mitophagy induced by PMA in PRKN-KO HeLa cells. ECAM^{+} WT, ECAM^{+} PRKN^{+} or ECAM^{+} PRKN-KO HeLa cells were incubated with PMA (0, 0.2 μM) for 6 h. These cells were visualized by confocal microscopy (C) and then measured for intracellular fluorescence intensity (D). M.F.I. per cell was quantified by imageJ, Data are presented as means ± SEM of three independent experiments. n = 20. ns, non-significant; *p ≤ 0.05 **p ≤ 0.01, ***p ≤ 0.001, ****p ≤ 0.0001 (t-test). Scale bars: 10 μm.

Serendipitously, we found that phorbol-12-myristate-13-acetate (PMA), an activator of PRKC/PKC (protein kinase C), potently triggered mitophagy in *PRKN*$^+$ HeLa cells at 1–10 nM concentrations Figure 8(A,B). We then examined PMA by ECAM in *PRKN*$^+$ as well as *PRKN*-KO HeLa cells. PMA elicited mitophagy about 2-fold greater in *PRKN*$^+$ HeLa cells over *PRKN*-KO and WT cells Figure 8(C,D), showing that PMA could induce mitophagy through both PINK1-PRKN pathway and PRKN-independent pathways. To our delight, PMA effectively induced mitophagy in WT cells and *PRKN*-KO cells at a concentration as low as 0.2 μM Figure 8(C,D), showing its superior performance over classical mitophagy inducers such as CCCP and rotenone Figure 7(A,B). PMA-elicited mitophagy was independently confirmed by western blotting on increased LC3A:LC3B ratio and decreased levels of TOMM20, a constituent mitochondrial membrane protein (Fig. S7A-B). These data further consolidate the utility of ECAM to discern mitophagy-inducing compounds.

Finally, we evaluated cytotoxicity and photostability of ECAM. ^{Az}Choline$^+$ HeLa cells were stained with varied doses of Mito-proGreen in DMEM for 0–48 h. No obvious detrimental effects could be observed on cell viability as determined by a cell count kit 8 assay (Fig. S8A). We next investigated photostability of ECAM. The solution of Mito-proGreen and LNPEP or starved ECAM$^+$ cells were subjected to continuous laser illumination. This revealed relatively constant fluorescence of Mito-Green generated in buffer as well as in live cells after 3 h and 1 h illumination (Fig. S8B and S8C). The observed high photostability and low cytotoxicity of ECAM are beneficial for long-term optical tracking of mitophagy.

Imaging of mitophagy is valuable to define the role of aberrant mitophagy in multiple diseases. Mitophagy has been imaged with synthetic or biotic pH sensors by reporting lysosomal acidity upon delivery into lysosomes. We previous immobilized an acidity-responsive probe inside mitochondria either by intra-organelle conjugation with another small molecular probe to give adducts of higher molecular weight or by conjugation with azidolipids in mitochondrial inner membrane [36,37]. Although being able to track stressed mitochondria, both approaches relied on lysosomal acidity to give mitophagy-reporting signals, and thus are inapplicable in fixed cells due to signal or probe loss from permeabilized lysosomes. We herein coined ECAM by anchoring an enzyme-activated probe with azidolipids metabolically incorporated into mitochondrial inner membrane. ECAM allows signal-persist mitophagy imaging in live cells and fixed cells, thus overcoming the liability of conventional acidity-based mitophagy imaging probe to signal interference by lysosomal pH changes and to dissipation upon cell fixation.

Conclusion

Imaging of mitophagy is of significance to investigate mitochondrial biology and mitophagy inducers. Albeit widely used, chemical or proteinaceous acidity-reporting probes are hampered by signal disturbance by lysosomal pH alteration. Mitophagy imaging via acidity-independent readout was recently achieved using a pair of fused fluorescent proteins: one degradable by lysosomal proteinases and the other remains intact and fluorescent in lysosomes [53]. Contrasting protein-based probes that require gene cloning and construction of transgenic cell lines, chemical probes could be applied exogenously to achieve culture-to-use imaging in diverse cell lines, but are prone to loss from stressed organelles or fixed cells. We herein report an enzyme-activated probe covalently anchored on mitochondrial membrane (ECAM) that enables mitophagy imaging by always-on fluorescence. ECAM utilizes a small molecular ΔΨm probe (Mito-proGreen) that promptly accumulates in mitochondria whereby it reacts with azidophospholipids metabolically installed on mitochondrial membrane, thus trapping the probe in mitochondria without resort to ΔΨm. Mitophagy leads to degradation of ECAM by leucyl amino peptidase in lysosomes, generating bright fluorescence insusceptible to lysosomal pH changes. Harnessing metabolic lipid labeling, ECAM overcomes the liability of classical chemical probes to dissipation from stressed organelles, and thus enables signal-sustained imaging of mitophagy and identification of PMA as a potent inducer of mitophagy. This approach integrates metabolic lipid labeling with organelle probes, providing a simplified and powerful tool to study mitophagy and significantly expanding the scope of chemical probes in bioimaging.

Materials and methods

Cell lines, plasmids and reagents

HeLa (CCL-2), NIH-3T3 (CRL-1658™), B16-F10 (CRL-6475™), MCF7 (HTB-22™), A549 (CCL-185), and HepG2 (HB-8065) were obtained from American Type Culture Collection. All cell lines were maintained in Dulbecco's modified Eagle's medium (DMEM; GIBCO, C11995500CP) containing 10% fetal bovine serum (Thermo, A3160901), 2 mM L-glutamine (Millipore, TMS-002-C), 100 IU penicillin (Gibco 15,140,122), and 100 mg/mL streptomycin (Sangon, A610494–0050) at 37°C in a humidified incubator under 5% CO_2, unless specified. Bafilomycin A_1 (Baf-A1, S1413), rapamycin (S1039) and oligomycin (S1478) were purchased from Selleck. Etoposide (E1383), and CCCP (C2759) were purchased from Sigma. Compounds **1–19** were prepared following an established procedure [62]. All other chemicals were purchased from Sigma unless specified. Antibody for LC3A/B (12741), PRKN/parkin (32833S) and ACTB/β-actin (3700S) were from Cell Signaling Technology. Antibody for ATG7 (67341) and ATG9A (67096) were from Proteintech. *PRKN*$^+$ HeLa cells were obtained as described in literature [36]. To obtain *ATG5*-KO, *ATG7*-KO, *ATG9A*-KO and *PRKN*-KO HeLa cells, the following targeting sequences were used to generate CRISPR-Cas9-mediated knockout HeLa cells according to the manual "LentiCRISPRv2 and lentiGuide-Puro: lentiviral CRISPR/Cas9 and single guide RNA" from Feng Zhang Lab at Harvard University.

sgATG5: 5'-GAACGTCAAATAACTTACTCT-3'
sgATG7: 5'-GAACTGCAGTTTAGAGAGTCC-3'
sgATG9A: 5'-GTATAGGAGGCCTCTAGGCGC-3'
sgPRKN: 5'-GTGTCAGAATCGACCTCCAC-3'

Microscopy and western blotting

The fluorescence spectra were performed on SpectraMax M5 (Molecular Device). All cell imaging assays were independently performed three times. Confocal fluorescence microscopy imaging was performed on Zeiss LSM 980 using the following filters: λ_{ex} = 488 nm/λ_{em} = 499–553 nm for GFP and Mito-proGreen, λ_{ex} = 543 nm/λ_{em} = 570–620 nm for ^{Az}Red, RFP and LysoTracker Red. λ_{ex} = 405 nm/λ_{em} = 415–480 nm for coumarin. λ_{ex} = 633 nm/λ_{em} = 640–680 nm for MtioTracker Deep Red. Images of merged fluorescence were processed using ZEN 3.4 (blue edition). The super-resolution imaging of mitochondria was performed by SIM-Ultimate(csr-biotech) using the following filters: λ_{ex} = 488 nm/λ_{em} = 499–553 nm for GFP, λ_{ex} = 561 nm/λ_{em} = 570–620 nm for ^{Az}Red. Obtained images were processed using SIM-Ultimate software. All the cells analyzed by confocal microscopy were seeded in 35 mm glass-bottom cell culture dishes purchased from NEST, Wuxi. Flow cytometry analysis was performed on BD Fortessa. The fluorescence emission intensity of Mito-proGreen was recorded by FITC filter (515–545 nm) using excitation wavelength of 488 nm while that of ^{Az}Red was recorded by PE (571–601 nm) using excitation wavelength of 561 nm. For flow cytometry 10,000 Cells were gated and analyzed under identical conditions. The data were processed by FlowJo V10. Graphs were generated by GraphPad Prism 8 software and Origin 9 software.

For western blotting, cells were harvested in lysis buffer containing 20 mM Tris-HCl (Sigma, V900483) (pH 7.4), 150 mM NaCl (Sigma,S5886), 1 mM EDTA (Sangon,A500895), 1 mM EGTA (Sigma,E3889), 1% Triton X-100 (Sangon, A110694), 2.5 mM sodium pyrophosphate (Sangon,SB0883), 1 mM β-glycerolphosphate (beyotime, ST637), 1 mM sodium orthovanadate (Sigma, S6508), 1 μg/ml leupeptin (Sigma, L2884), and 1 mM phenylmethylsulfonyl fluoride (MCE, HY-B0496). Insoluble cell fraction was separated by centrifugation at 12,000 g for 10 min at 4°C and the supernatant were boiled in SDS-PAGE loading buffer for 10 min. Proteins in total cell lysates were separated by SDS-PAGE and transferred to PVDF membranes. Membranes were blocked in 5% nonfat milk (beyotime, P0216) or BSA (beyotime, ST2254) and incubated with the appropriate primary antibodies (as aforementioned). Protein bands were visualized on a Fujifilm LAS-4000 imager through horseradish peroxidase (HRP)-conjugated secondary antibodies (Invitrogen, Goat anti-Human IgG (H+L), 31410; Mouse anti-Human IgG1 Fc, A-10648) using ECL A and ECL B reagents (beyotime, P0018M).

Statistical evaluation

Confocal fluorescence microscopy images were used for measurement of mean fluorescence intensity (M.F.I.). 20 Cells were analyzed and fluorescence intensity per cell was quantified by imageJ software. Statistical analysis was performed with Prism software (GraphPad Software) for. Data are presented as the means ± SEM. Unpaired two-tailed Student's t-test was used to compare differences between treated groups and their paired controls. Differences in compared groups with p values lower than 0.05 were considered statistically significant. ns, non-significant; *$p \le 0.05$, **$p \le 0.01$; ***$p \le 0.001$; ****$p \le 0.0001$.

Screening of LNPEP for ECAM

HeLa, NIH-3T3, B16-F10, and MCF7 cells were cultured for 1 h in DMEM containing compounds **1–19** or no addition (10 μM) at 37°C. The cells were washed with PBS (Thermo, AM9624), and then analyzed by flow cytometry. HeLa cells were cultured for 1 h with compound **10** (2 μM), washed with PBS for three times, and then stained with LysoTracker Red (1 μM, 1 h) (Thermo, L12492). The cells were washed with PBS for three times and then analyzed by confocal fluorescence microscopy.

pH titration

The solution of Mito-proGreen (10 μM) or Ac-Mito-proGreen (10 μM) in PBS (137.0 mM NaCl, 2.7 mM KCl, 10 mM Na_2HPO_4, 2.0 mM KH_2PO_4) of pH 4.5 or 8.0 containing 10% dimethyl sulfoxide (DMSO; Sigma, D5879–1 L) was analyzed for fluorescence emission using λ_{ex} = 520 nm. For parent fluorophore, a stock solution of compound **S4** (10 μM) in PBS containing 10% DMSO of different pH (4.0, 4.5, 5.0, 5.5, 6.0, 6.5, 7.0, 7.5, 8.0, 8.5, 9.0) was detected for fluorescence emission (λ_{ex} = 520 nm).

Mito-proGreen activation by LNPEP

Probe activation by LNPEP: To the solution of Mito-proGreen (10 μM) in PBS (10 mM, pH = 7.4) containing 10% DMSO was added LNPEP (0.5 mg/mL, TargetMol, T9345–50 mg). The mixture was incubated at 37°C for 0–180 min and then analyzed for fluorescence emission at different time after incubation. For comparison, To PBS (10 mM, pH = 7.4) containing LNPEP (0.5 mg/mL) was added Mito-proGreen (10 μM) or Ac-Mito-proGreen (10 μM). The solution was incubated at 37°C for 1 h and then analyzed for fluorescence emission. The solution of Mito-proGreen (2 μM) and LNPEP (1 mg/mL) in PBS (10 mM, pH = 7.4) containing 10% DMSO was maintained at 37°C for 1 h and then analyzed by MALDI-TOF MS.

Dose-dependent activation: To the solution of Mito-proGreen (10 μM) in PBS (10 mM, pH = 7.4) containing 10% DMSO was added LNPEP (0, 0.025, 0.05, 0.1, 0.25, 0.5 and 1.0 mg/mL). The solution was incubated at 37°C for 1 h and then analyzed for fluorescence emission.

Bestatin-inhibited activation: To the solution of Mito-proGreen (10 μM) and LNPEP (0.5 mg/mL) in PBS (10 mM, pH = 7.4) containing 10% DMSO, was added Bestatin (Beyotime, SG2008-25 mg) (0 mM, 0.1 mM, 0.2 mM, 0.3 mM, 0.4 mM or 0.5 mM). The solution was incubated at 37°C for 6 h, and then analyzed for fluorescence emission.

Selectivity of Mito-proGreen for mitochondria

Dose-dependent retention of ^{Az}Red in Mito-proGreen^{+} ^{Az}Red^{+} HeLa cells: ^{Az}Red was prepared following a reported literature [42]. HeLa cells were cultured for 1 h with ^{Az}Red (0.2 μM), washed with PBS for three times and then

cultivated for 1 h in DMEM containing Mito-proGreen (0, 1, 2, or 5 μM). Cells were washed with PBS for three times and then maintained for 1 h in DMEM containing CCCP (30 μM) or no addition. The cells were analyzed by confocal microscopy without washing.

Retention of ^{Az}Red in Mito-proGreen$^+$ HeLa cells: ^{Az}Red$^+$ Hela cells were treated with Mito-proGreen (2 μM, 1 h), washed with PBS for three times, and then stained with MitoTracker Deep Red (MTDR, 0.2 μM, 15 min; MCE, HY-D1783). The cells were washed with PBS for three times, maintained for 1 h in DMEM containing CCCP (30 μM) and then imaged by confocal microscopy without washing.

Retention of ^{Az}Red in ^{Az}Red$^+$ Mito-proGreen$^+$ TOMM20-GFP$^+$ HeLa cells. TOMM20-GFP$^+$ HeLa cells were cultured for 1 h with ^{Az}Red (0.2 μM), washed with PBS for three times and then cultivated for 1 h in DMEM containing Mito-proGreen (2 μM). The cells were further maintained in DMEM containing CCCP (30 μM) or no addition for 1 h, and then imaged by SIM-Ultimate without washing.

Fidelity of ECAM for mitophagy

ATG5-dependent activation of ECAM. WT or *ATG5*-KO HeLa cells were cultured in DMEM containing ^{Az}choline (0, 500 μM) for 24 h. The cells were washed with PBS for three times and then cultured with Mito-proGreen (2 μM) for 1 h. The cells (defined as ECAM$^+$ cells) were cultivated in fresh DMEM (0 h, 6 h) and then imaged by confocal microscopy.

Detection of starvation-induced mitophagy. ECAM$^+$ WT HeLa cells or ECAM$^+$ *ATG5*-KO HeLa cells were maintained for 6 h in fresh DMEM (control) or HBSS, and then analyzed by confocal microscopy.

Detection of PRKN-augmented mitophagy. ECAM$^+$ WT HeLa cells or ECAM$^+$ *PRKN*$^+$ HeLa cells were incubated in DMEM containing CCCP (0, 10 μM) for 6 h and then analyzed by confocal microscopy without washing.

Detection of mitophagy of stressed mitochondria. Mito-proGreen$^+$ HeLa cells or ECAM$^+$ HeLa cells were independently incubated with CCCP (0, 30 μM) in DMEM for 1 h, and then washed with PBS for three times. The cells were maintained for 6 h in fresh DMEM or HBSS and then analyzed without washing by confocal microscopy.

Lysosomal activation of ECAM. ECAM$^+$ WT HeLa cells pre-stained with LysoTracker Red (1 μM, 1 h) were washed with PBS for three times, and then maintained for 6 h in DMEM or HBSS. These cells were analyzed without washing by confocal microscopy. In parallel, ECAM$^+$ LAMP2-GFP HeLa cells were maintained for 6 h in fresh DMEM or HBSS and then analyzed by confocal microscopy without washing.

ECAM activation by LNPEP in live cells

Incapability of LNPEP to activate Ac-Mito-proGreen. ^{Az}Choline$^+$ HeLa cells were stained with Ac-Mito-proGreen (2 μM, 1 h), washed three times with PBS, and then maintained for 6 h in fresh DMEM or HBSS. The cells were analyzed without washing by confocal microscopy.

ECAM$^+$ WT HeLa, ECAM$^+$ HepG2 cells and ECAM$^+$ A549 cells were independently maintained for 6 h in fresh DMEM or HBSS and then analyzed without washing by confocal microscopy.

Signal-sustained mitophagy imaging with ECAM

Lysosomal pH-inert fluorescence from ECAM. ECAM$^+$ WT HeLa cells or ^{Az}choline$^+$ ^{DBCO}RC-TPP$^+$ HeLa cells [37] were maintained for 6 h in fresh DMEM, HBSS, or HBSS spiked with bafilomycin A_1 (Baf-A1, 50 nM) and then analyzed by confocal microscopy.

Retention of green signals from ECAM in fixed cells. ECAM$^+$ HeLa cells or Mito-proGreen$^+$ HeLa cells were maintained for 6 h in HBSS, washed with PBS for three times, and then incubated with PBS (1 mL, control) or paraformaldehyde at room temperature for 15 min. The cells were washed again and then analyzed by confocal microscopy.

Time course analysis on mitophagy-mediated ECAM activation

ECAM$^+$ WT HeLa cells were maintained in HBSS for 0–6 h. At 0 h, 2 h, 4 h, and 6 h post-incubation, the cells were visualized by confocal microscopy.

ECAM$^+$ *PRKN*$^+$ HeLa cells were incubated with CCCP (30 μM) in DMEM for 0–6 h. At 0 h, 2 h, 4 h, and 6 h post-incubation, the cells were analyzed by confocal microscopy without washing.

Discern of mitophagy-inducers with ECAM

PMA-induced mitophagy in *PRKN*$^+$ cells. ECAM$^+$ PRKN$^+$ HeLa cells were cultured with CCCP (10 μM; MCE, HY-100941), etoposide (10 μM; Sigma, E1383), oligomycin (10 μM; MCE, HY-N6782), rapamycin (10 μM; MCE, HY-10219), rotenone (10 μM; Sigma, R8875) or no addition for 6 h in DMEM, and then analyzed by confocal microscopy without washing. For PMA: ECAM$^+$ *PRKN*$^+$ HeLa cells were maintained in fresh DMEM (control), or DMEM spiked with varied levels of PMA (1 nM, 10 nM, 0.2 μM and 0.5 μM) for 6 h, then washed three times with PBS and analyzed by confocal microscopy.

PMA-induced mitophagy in *PRKN*-KO cells. ECAM$^+$ WT, ECAM$^+$ *PRKN*$^+$ and ECAM$^+$ *PRKN*-KO HeLa cells were maintained in fresh DMEM (control), or DMEM spiked with PMA (0.2 μM) for 6 h, then washed three times with PBS and analyzed by confocal microscopy.

Cytotoxicity and photostability of ECAM

Cytotoxicity: HeLa cells were cultured in DMEM containing ^{Az}choline (500 μM) for 24 h, washed with PBS for three times and then stained with Mito-proGreen (0, 2, 5, 10 μM) in a 96-well cell culture plate for 1 h. The cells were washed with PBS for three times and then further cultured in fresh DMEM for 0 h, 24 h, or 48 h. The cells were determined for cell viability and cell number by cell count kit 8 (MCE, hy-k0301) assay ($n = 3$).

Photostability: The solution of Mito-proGreen (2 μM) in PBS (10 mM, pH 7.4) containing DMSO (10% v/v)

preincubated with LNPEP (0.5 mg/mL) for 1 h was subjected to constant Laser irradiation for 3 h and then recorded for fluorescence emission at λ_{em} = 555 nm using λ_{ex} = 520 nm. For intracellular photostability, starved ECAM$^+$ cells were irradiated under constant laser for 1 h. During irradiation, the cells were imaged at every other 10 min with a confocal fluorescence microscope (λ_{ex} = 488 nm).

Disclosure statement

No potential conflict of interest was reported by the author(s).

Funding

This work was supported by grants from National Natural Science Foundation of China (NSFC) [No. 22177096, 82388201], National Key R&D Program of China [2020YFA0803500], and the CAMS Innovation Fund for Medical Science (2019-I2M-5-062). We thank Narong Yang for helpful discussion.

Supporting information

available on synthesis and characterization of chemical probes, cell cytotoxicity of ECAM, western blotting on mitophagy verification, cell imaging on subcellular location of ECAM signals, etc.

references

[1] Wang L, Qi H, Tang Y, et al. Post-translational modifications of key machinery in the control of mitophagy. Trends Biochem Sci. 2020;45(1):58–75. doi: 10.1016/j.tibs.2019.08.002
[2] Ashrafi G, Schwarz TL. The pathways of mitophagy for quality control and clearance of mitochondria. Cell Death Differ. 2013;20 (1):31–42. doi: 10.1038/cdd.2012.81
[3] Kubli DA, Gustafsson AB. Mitochondria and mitophagy: the YAn and Yang of cell death control. Circ Res. 2012;111(9):1208–1221. doi: 10.1161/CIRCRESAHA.112.265819
[4] Panigrahi DP, Praharaj PP, Bhol CS, et al. The emerging, multifaceted role of mitophagy in cancer and cancer therapeutics. Semin Cancer Biol. 2020;66:45–58. doi: 10.1016/j.semcancer.2019.07.015
[5] Chen W, Zhao H, Li Y. Mitochondrial dynamics in health and disease: mechanisms and potential targets. Signal Transduct Target Ther. 2023;8(1):333. doi: 10.1038/s41392-023-01547-9
[6] Harrington JS, Ryter SW, Plataki M, et al. Mitochondria in health, disease, and aging. Physiol Rev. 2023;103(4):2349–2422. doi: 10.1152/physrev.00058.2021
[7] Mito T, Vincent AE, Faitg J, et al. Mosaic dysfunction of mitophagy in mitochondrial muscle disease. Cell Metab. 2022;34 (2):197–208.e5. doi: 10.1016/j.cmet.2021.12.017
[8] Wang S, Long H, Hou L, et al. The mitophagy pathway and its implications in human diseases. Signal Transduct Target Ther. 2023;8(1):304. doi: 10.1038/s41392-023-01503-7
[9] Doblado L, Lueck C, Rey C, et al. Mitophagy in human diseases. Int J Mol Sci. 2021;22(8):3903. doi: 10.3390/ijms22083903
[10] Eldeeb MA, Thomas RA, Ragheb MA, et al. Mitochondrial quality control in health and in Parkinson's disease. Physiol Rev. 2022;102 (4):1721–1755. doi: 10.1152/physrev.00041.2021
[11] Dong Y, Zhuang X-X, Wang Y-T, et al. Chemical mitophagy modulators: drug development strategies and novel regulatory mechanisms. Pharmacol Res. 2023;194:106835. doi: 10.1016/j.phrs.2023.106835
[12] Georgakopoulos ND, Wells G, Campanella M. The pharmacological regulation of cellular mitophagy. Nat Chem Biol. 2017;13 (2):136–146. doi: 10.1038/nchembio.2287
[13] Xie C, Zhuang X-X, Niu Z, et al. Amelioration of Alzheimer's disease pathology by mitophagy inducers identified via machine learning and a cross-species workflow. Nat Biomed Eng. 2022;6 (1):76–93. doi: 10.1038/s41551-021-00819-5
[14] Ding S, Hong Y. The fluorescence toolbox for visualizing autophagy. Chem Soc Rev. 2020;49(22):8354–8389. doi: 10.1039/D0CS00913J
[15] Ma D, Huang C, Zheng J, et al. Azoreductase-responsive nanoprobe for hypoxia-induced mitophagy imaging. Anal Chem. 2018;91(2):1360–1367. doi: 10.1021/acs.analchem.8b03492
[16] Liu Y, Zhou J, Wang L, et al. A cyanine dye to probe mitophagy: simultaneous detection of mitochondria and autolysosomes in live cells. J Am Chem Soc. 2016;138(38):12368–12374. doi: 10.1021/jacs.6b04048
[17] Gui L, Yuan Z, Kassaye H, et al. A tumor-targeting probe based on a mitophagy process for live imaging. Chem Commun (Camb). 2018;54(69):9675–9678. doi: 10.1039/C8CC04246B
[18] Liu Y, Teng L, Chen L, et al. Engineering of a near-infrared fluorescent probe for real-time simultaneous visualization of intracellular hypoxia and induced mitophagy. Chem Sci. 2018;9 (24):5347–5353. doi: 10.1039/C8SC01684D
[19] Li X, Liang X, Yin J, et al. Organic fluorescent probes for monitoring autophagy in living cells. Chem Soc Rev. 2021;50 (1):102–119. doi: 10.1039/D0CS00896F
[20] Munan S, Kottarathil S, Joseph MM, et al. IndiFluors: a new full-visible color-tunable donor-acceptor-donor (D(1)-A-D(2)) fluorophore family for ratiometric pH imaging during mitophagy. ACS Sens. 2022. doi: 10.1021/acssensors.1c02381
[21] Kimura S, Noda T, Yoshimori T. Dissection of the autophagosome maturation process by a novel reporter protein, tandem fluorescent-tagged LC3. Autophagy. 2007;3(5):452–460. doi: 10.4161/auto.4451
[22] Kaizuka T, Morishita H, Hama Y, et al. An autophagic flux probe that releases an internal control. Mol Cell. 2016;64(4):835–849. doi: 10.1016/j.molcel.2016.09.037
[23] Rosado C, Mijaljica D, Hatzinisiriou I, et al. Rosella: A fluorescent pH-biosensor for reporting vacuolar turnover of cytosol and organelles in yeast. Autophagy. 2008;4(2):205–213. doi: 10.4161/auto.5331
[24] Katayama H, Kogure T, Mizushima N, et al. A sensitive and quantitative technique for detecting autophagic events based on lysosomal delivery. Chem Biol. 2011;18(8):1042–1052. doi: 10.1016/j.chembiol.2011.05.013
[25] Ye Z, Wei L, Geng X, et al. Mitochondrion-specific blinking fluorescent bioprobe for nanoscopic monitoring of mitophagy. ACS Nano. 2019;13(10):11593–11602. doi: 10.1021/acsnano.9b05354
[26] Zhu H, Fan J, Du J, et al. Fluorescent probes for sensing and imaging within specific cellular organelles. Acc Chem Res. 2016;49(10):2115–2126. doi: 10.1021/acs.accounts.6b00292
[27] Niu G, Liu W, Wu J, et al. Aminobenzofuran-fused rhodamine dyes with deep-red to near-infrared emission for biological applications. J Org Chem. 2015;80(6):3170–3175. doi: 10.1021/acs.joc.5b00077
[28] Lee MH, Park N, Yi C, et al. Mitochondria-immobilized ph-sensitive off–on fluorescent probe. J Am Chem Soc. 2014;136 (40):14136–14142. doi: 10.1021/ja506301n
[29] Wu X, Fu G, Li Y, et al. Dihydroxanthene-based near-infrared fluorescent probes for monitoring mitochondrial viscosity in living cells and mice. Anal Chem. 2023;95(6):3544–3549. doi: 10.1021/acs.analchem.2c05713
[30] Li X, Hu Y, Li X, et al. Mitochondria-immobilized near-infrared ratiometric fluorescent ph probe to evaluate cellular mitophagy. Anal Chem. 2019;91(17):11409–11416. doi: 10.1021/acs.analchem.9b02782
[31] Iwashita H, Torii S, Nagahora N, et al. Live cell imaging of mitochondrial autophagy with a novel fluorescent small molecule. ACS Chem Biol. 2017;12(10):2546–2551. doi: 10.1021/acschembio.7b00647
[32] Wang X, Fan L, Wang S, et al. Real-time monitoring mitochondrial viscosity during mitophagy using a mitochondria-immobilized near-infrared aggregation-induced emission probe. Anal Chem. 2021;93(6):3241–3249. doi: 10.1021/acs.analchem.0c04826

[33] Leung CWT, Hong Y, Chen S, et al. A photostable AIE luminogen for specific mitochondrial imaging and tracking. J Am Chem Soc. 2012;135(1):62–65. doi: 10.1021/ja310324q

[34] Jin C, Liu J, Chen Y, et al. Cyclometalated Iridium(III) complexes as AIE Phosphorescent probes for real-time monitoring of mitophagy in living cells. Sci Rep. 2016;6(1). doi: 10.1038/srep22039

[35] Hu F, Cai X, Manghnani PN, et al. Multicolor monitoring of cellular organelles by single wavelength excitation to visualize the mitophagy process. Chem Sci. 2018;9(10):2756–2761. doi: 10.1039/C7SC04585A

[36] Shi Y, Zou X, Wen S, et al. An organelle-directed chemical ligation approach enables dual-color detection of mitophagy. Autophagy. 2021;17(11):3475–3490. doi: 10.1080/15548627.2021.1875597

[37] Wen S, Hu X, Shi Y, et al. Imaging of mitophagy enabled by an acidity-reporting probe anchored on the mitochondrial inner membrane. Anal Chem. 2021;93(50):16887–16898. doi: 10.1021/acs.analchem.1c03881

[38] Ross MF, Kelso GF, Blaikie FH, et al. Lipophilic triphenylphosphonium cations as tools in mitochondrial bioenergetics and free radical biology. Biochemistry (Moscow). 2005;70(2):222–230. doi: 10.1007/s10541-005-0104-5

[39] Smith RAJ, Hartley RC, Murphy MP. Mitochondria-targeted small molecule therapeutics and probes. Antioxid Redox Signaling. 2011;15(12):3021–3038. doi: 10.1089/ars.2011.3969

[40] Ross Meredith F, Prime Tracy A, Abakumova I, et al. Rapid and extensive uptake and activation of hydrophobic triphenylphosphonium cations within cells. Biochem J. 2008;411(3):633–645. doi: 10.1042/BJ20080063

[41] Ross Meredith F, Da Ros T, Blaikie Frances H, et al. Accumulation of lipophilic dications by mitochondria and cells. Biochem J. 2006;400(1):199–208. doi: 10.1042/BJ20060919

[42] Jiang F, Shi Y, Zou X, et al. In cellulo synthesis of dendrimeric sensors for fluorescence-on imaging of bacterial phagocytosis. J Mat Chem B. 2022;10(25):4800–4809. doi: 10.1039/D1TB02012A

[43] Heytler PG. uncoupling of oxidative phosphorylation by carbonyl cyanide phenylhydrazones. I. Some characteristics of m-Cl-CCP action on mitochondria and chloroplasts. Biochemistry. 1963;2(2):357–361. doi: 10.1021/bi00902a031

[44] Cai Q, Jeong YY. Mitophagy in Alzheimer's disease and other age-related neurodegenerative diseases. Cells. 2020;9(1):150. doi: 10.3390/cells9010150

[45] Liu J, Liu W, Li R, et al. Mitophagy in Parkinson's Disease: From pathogenesis to treatment. Cells. 2019;8(7):712. doi: 10.3390/cells8070712

[46] Jao CY, Roth M, Welti R, et al. Biosynthetic labeling and two-color imaging of phospholipids in cells. Chembiochem. 2015;16(3):472–476. doi: 10.1002/cbic.201402149

[47] Tamura T, Fujisawa A, Tsuchiya M, et al. Organelle membrane-specific chemical labeling and dynamic imaging in living cells. Nat Chem Biol. 2020;16(12):1361–1367. doi: 10.1038/s41589-020-00651-z

[48] D-E S, Fan X, Shi Y, et al. Click-ExM enables expansion microscopy for all biomolecules. Nat Methods. 2020;18(1):107–113. doi: 10.1038/s41592-020-01005-2

[49] Correia-Melo C, Ichim G, Tait S, et al. Depletion of mitochondria in mammalian cells through enforced mitophagy. Nat Protocols. 2017;12(1):183–194. doi: 10.1038/nprot.2016.159

[50] Soutar MPM, Kempthorne L, Annuario E, et al. FBS/BSA media concentration determines CCCP's ability to depolarize mitochondria and activate PINK1-PRKN mitophagy. Autophagy. 2019;15(11):2002–2011. doi: 10.1080/15548627.2019.1603549

[51] Gong Q, Shi W, Li L, et al. Leucine aminopeptidase may contribute to the intrinsic resistance of cancer cells toward cisplatin as revealed by an ultrasensitive fluorescent probe. Chem Sci. 2016;7(1):788–792. doi: 10.1039/C5SC03600C

[52] Yoshimori T, Yamamoto A, Moriyama Y, et al. Bafilomycin A1, a specific inhibitor of vacuolar-type H(+)-ATPase, inhibits acidification and protein degradation in lysosomes of cultured cells. J Biol Chem. 1991;266(26):17707–17712. doi: 10.1016/S0021-9258(19)47429-2

[53] Katayama H, Hama H, Nagasawa K, et al. Visualizing and modulating mitophagy for therapeutic studies of neurodegeneration. Cell. 2020;181(5):1176–87.e16. doi: 10.1016/j.cell.2020.04.025

[54] Nunnari J, Suomalainen A. Mitochondria: in sickness and in health. Cell. 2012;148(6):1145–1159. doi: 10.1016/j.cell.2012.02.035

[55] Andreux PA, Houtkooper RH, Auwerx J. Pharmacological approaches to restore mitochondrial function. Nat Rev Drug Discov. 2013;12(6):465–483. doi: 10.1038/nrd4023

[56] Harrison DE, Strong R, Sharp ZD, et al. Rapamycin fed late in life extends lifespan in genetically heterogeneous mice. Nature. 2009;460(7253):392–395. doi: 10.1038/nature08221

[57] Alvers AL, Wood MS, Hu D, et al. Autophagy is required for extension of yeast chronological life span by rapamycin. Autophagy. 2009;5(6):847–849. doi: 10.4161/auto.8824

[58] Graziotto JJ, Cao K, Collins FS, et al. Rapamycin activates autophagy in Hutchinson-Gilford progeria syndrome: implications for normal aging and age-dependent neurodegenerative disorders. Autophagy. 2012;8(1):147–151. doi: 10.4161/auto.8.1.18331

[59] Li Q, Gao S, Kang Z, et al. Rapamycin enhances mitophagy and attenuates apoptosis after spinal ischemia-reperfusion injury. Front Neurosci. 2018;12:865. doi: 10.3389/fnins.2018.00865

[60] Bang M, Kim DG, Gonzales EL, et al. Etoposide induces mitochondrial dysfunction and cellular senescence in primary cultured rat astrocytes. Biomolecules & Ther. 2019;27(6):530–539. doi: 10.4062/biomolther.2019.151

[61] Custodio JB, Cardoso CM, Madeira VM, et al. Mitochondrial permeability transition induced by the anticancer drug etoposide. Toxicol In Vitro. 2001;15(4–5):265–270. doi: 10.1016/S0887-2333(01)00019-4

[62] Sinclair A, Mulcahy LE, Geldeard L, et al. Development of an in situ culture-free screening test for the rapid detection of Staphylococcus aureus within healthcare environments. Org Biomol Chem. 2013;11(20):3307. doi: 10.1039/c3ob40150b